Publ. Astron. Soc. Japan (2016) 68 (4), 63 (1–8)
doi: 10.1093/pasj/psw062
Advance Access Publication Date: 2016 June 30

Three-dimensional distribution of the ISM in the Milky Way Galaxy. IV. 3D molecular fraction and Galactic-scale H I-to-H_2 transition

Yoshiaki Sofue[1,*] and Hiroyuki Nakanishi[2,3]

[1]Insitute of Astronomy, The University of Tokyo, 2-21-1 Osawa, Mitaka, Tokyo 181-0015, Japan
[2]Graduate Schools of Science and Engineering, Kagoshima University, 1-21-35 Korimoto, Kagoshima, Kagoshima 890-8544, Japan
[3]Institute of Space and Astronautical Science, Japan Aerospace Exploring Agency, 3-1-1 Yoshinodai, Sagamihara, Kanagawa 252-5210, Japan

*E-mail: sofue@ioa.s.u-tokyo.ac.jp

Received 2016 March 11; Accepted 2016 May 14

Abstract

Three-dimensional (3D) distribution of the volume-density molecular fraction, defined by $f^{\rho}_{\rm mol} = \rho_{\rm H_2}/(\rho_{\rm H\,I} + \rho_{\rm H_2})$, is studied in the Milky Way Galaxy. The molecular front appears at galacto-centric distance of $R \sim 8$ kpc, where the galactic-scale phase transition from atomic to molecular hydrogen occurs with $f^{\rho}_{\rm mol}$ dropping from ∼0.8 to 0.2 within a radial interval as narrow as ∼0.5 kpc. The $f^{\rho}_{\rm mol}$ front is much sharper than that of the surface density molecular fraction. The $f^{\rho}_{\rm mol}$ front also appears in the direction vertical to the galactic plane with a full width of the high-$f^{\rho}_{\rm mol}$ disk to be ∼100 pc. The radial and vertical $f^{\rho}_{\rm mol}$ profiles, particularly the front behavior, are fitted by theoretical curves calculated using the observed density profile and assumed radiation field and metallicity with exponential gradients. The molecular fraction was found to be enhanced along spiral arms at radii $R \sim 6$ to 10 kpc, such as the Perseus arm. This implies that the molecular clouds are produced from H I in the arms and are dissociated in the interarm regions in the transition region around the molecular front. We also show that there is a threshold value of mean H I density, over which H I is transformed into molecular gas.

Key words: Galaxy: general — ISM: atoms — ISM: general — ISM: molecules — ISM: structure — radio lines: ISM

1 Introduction

The atomic (H I) and molecular (H_2) hydrogen gases are the major constituents of the interstellar gas. The H_2 gas is dominant in the inner Galaxy, while H I is dominant in the outer Galaxy. The phase transition from H I to H_2 gases is determined by the environmental circumstances in the Galaxy, such as the pressure or the density, radiation field and the metallicity. The molecular fraction, the ratio of molecular to total gas densities, is one of the fundamental quantities for representing the ISM conditions (Elmegreen 1993; Krumholz et al. 2009).

Galactic-scale variation of the molecular fraction has been studied in the Galaxy and nearby galaxies using H I and CO line observational data (Sofue et al. 1995; Honma et al. 1995; Imamura & Sofue 1997; Hidaka & Sofue 2002; Nakanishi et al. 2006; Tosaki et al. 2011; Tanaka et al. 2014; Koda et al. 2016; Nakanishi & Sofue 2016). It was found that the molecular fraction is close to unity in the central regions, and decreases toward the outer galaxy. The

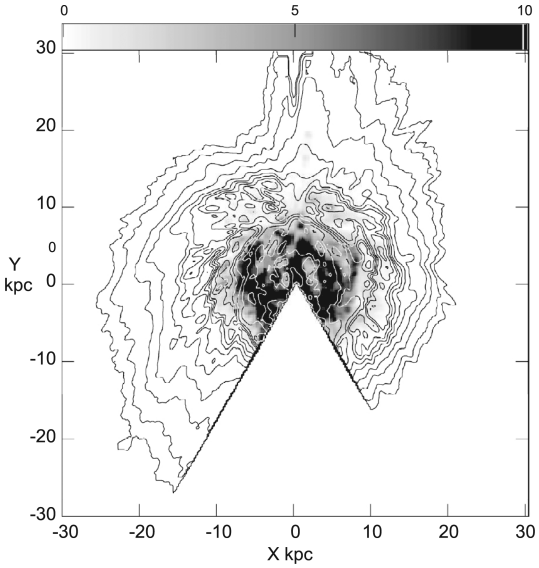

Fig. 1. H I (contours at 0.5 × 1, 2, 5,10, 20, 30, ... K km s^{-1}) and H_2(gray from 0 to 10 K km s^{-1}) face-on integrated intensity maps for a region at $-30 \leq X \leq +30$ kpc and $-30 \leq Y \leq +30$ kpc.

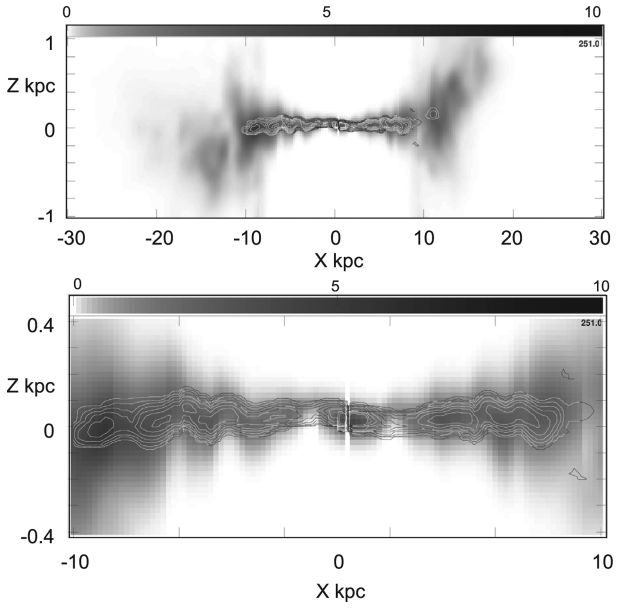

Fig. 2. H I (gray) and H_2(contour) cross-section at $Y = 0$ kpc for $-30 \leq X \leq +30$ kpc; $-1 \leq Z \leq +1$ kpc (top); and close up for $-10 \leq X \leq +10$ kpc; $-0.4 \leq Z \leq +0.4$ kpc. H I density is in gray scale as indicated by the bar (0 to 10 H cm^{-3}), and molecular density is shown by contours at 1, 2, 4, 8, 16, 32, ... H cm^{-3} ($= 2N_{H_2}$). Note that the Z scale is enlarged by 2.5 times the X-axis.

transition of the gaseous phases from H_2 to H I occurs in a relatively narrow galactocentric region called the molecular front.

In the current studies, observational molecular fraction has been represented in terms of the surface densities (column densities) of H I and H_2 gases. In order to compare with the theoretical analyses, it is more appropriate to measure the quantities in terms of volume densities. In this paper we derive the volume-density molecular fraction in the Milky Way Galaxy, and investigate its three-dimensional (3D) distribution using the H I and H_2 density cubes obtained by Nakanishi and Sofue (2003, 2006, 2016). The data cubes had 501 × 501 × 201 grids with increments of 200, 200, and 20 pc in the X-, Y- (in the galactic plane), and Z- (vertical to the plane) directions, respectively, covering a volume of 100 × 100 × 4 kpc^3 of the Galaxy.

2 3D molecular fraction

2.1 3D distributions of H I and H_2 gases

Figure 1 shows the distribution of integrated intensities of H I and CO ($J = 1$–0) line emissions ($I_{\rm HI}$ and $I_{\rm CO}$, respectively) projected on to the galactic plane (Nakanishi & Sofue 2016). They are proportional to the column densities of neutral hydrogen H and H_2 molecules $N_{\rm H}$ and $N_{\rm H_2}$, which are given by $N_{\rm H} = X_{\rm HI} I_{\rm HI}$ and $N_{\rm H_2} = X_{\rm CO} I_{\rm CO}$. Here, $X_{\rm HI} = 1.82 \times 10^{18}$ cm^{-2}(K km s^{-1})$^{-1}$ is the conversion factor of the H I intensity to H atom column density. The CO-to-H_2 conversion factor has been obtained from various analyses of emprical relations (Bottalo et al. 2013), and is converged to around $X_{\rm CO} \simeq 2 \times 10^{20}$ cm^{-2}(K km s^{-1})$^{-1}$. In this paper, we adopt $X_{\rm CO} = 1.8 \times 10^{20}$ cm^{-2}(K km s^{-1})$^{-1}$ following Dame et al. (2001).

Figure 2 shows meridional cross-sections of the gas disk across the Galactic center showing the volume densities $n_{\rm HI}$ and $n_{\rm H_2}$ in the (X, Z) plane (Nakanishi & Sofue 2016). The molecular gas is distributed in a thin and dense disk near the galactic plane, embedded in the broader and more extended H I disk.

2.2 3D molecular fraction

The surface-density (column density) molecular fraction is defined by

$$f^{\Sigma}_{\rm mol} = \frac{\Sigma_{\rm H_2}}{\Sigma_{\rm HI} + \Sigma_{\rm H_2}} = \frac{2N_{\rm H_2}}{N_{\rm HI} + 2N_{\rm H_2}}, \quad (1)$$

where $\Sigma_{\rm HI}$ and $\Sigma_{\rm H_2}$ are the surface mass densities of neutral hydrogen and molecular gases, respectively, integrated in the direction perpendicular to the galactic plane.

The volume-density molecular fraction is defined by

$$f^{\rho}_{\rm mol} = \frac{\rho_{\rm H_2}}{\rho_{\rm HI} + \rho_{\rm H_2}} = \frac{2n_{\rm H_2}}{n_{\rm HI} + 2n_{\rm H_2}}, \quad (2)$$

where $\rho_{\rm HI}$ and $\rho_{\rm H_2}$ are the volume densities of the H I and molecular hydrogen gases, and $n_{\rm HI}$ and $n_{\rm H_2}$ are the volume number densities, respectively.

In our previous paper (Nakanishi & Sofue 2016), we constructed H I and H_2 density cubes by applying the

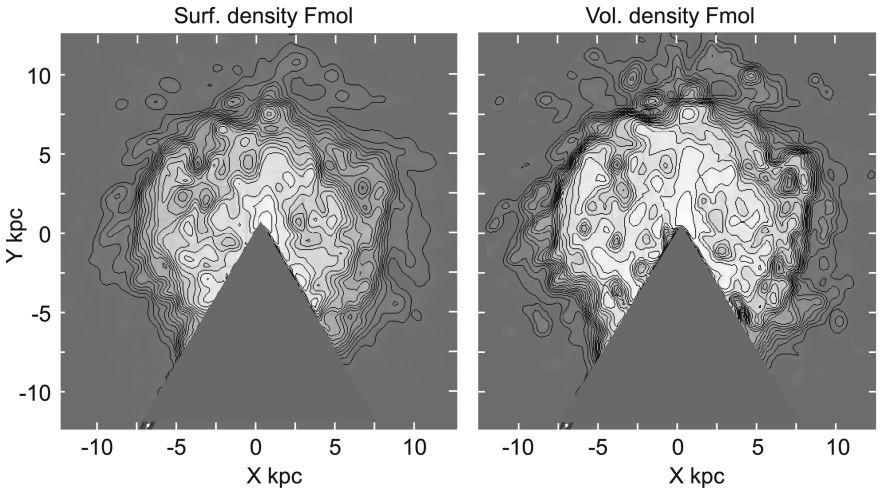

Fig. 3. (Left) Surface density molecular fraction $f^{\Sigma}_{\rm mol}$ in the (X, Y) plane. Contour interval is 0.1. The contours are drawn at every $\Delta f^{\Sigma}_{\rm mol} = 0.1$ starting from 0.1 with according gray scales. (Right) Same as left-hand panel, but for the volume density molecular fraction $f^{\rho}_{\rm mol}$ at $Z = 0$ kpc in the (X, Y) plane. The contours are drawn at every $\Delta f^{\rho}_{\rm mol} = 0.1$ starting from 0.1 with according gray scales.

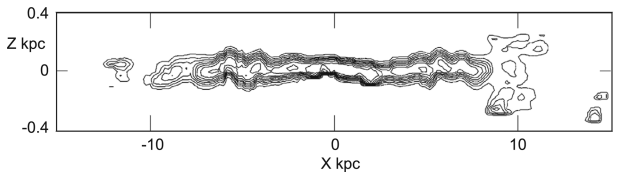

Fig. 4. (X, Z) cross-section of the 3D density molecular fraction $f^{\rho}_{\rm mol}$ at $Y = 0$. Contours are drawn at every $\Delta f^{\rho}_{\rm mol} = 0.1$ starting from 0.1.

velocity-to-space transformation to the kinematical data (line brightness temperature, local standard of rest velocity, galactic longitude and latitude) of H I- and CO-line spectral data using a galactic rotation curve assuming circular rotation of the Galaxy. Thereby, we used the Leiden–Argentine–Bonn (LAB) All Sky H I Survey (Kalberla et al. 2005) and the Colombia Galactic Plane CO-Line Survey (Dame et al. 2001). Using the thus-obtained density cubes, we constructed a 3D cube of the surface- and volume-density molecular fractions, $f^{\Sigma}_{\rm mol}$ and $f^{\rho}_{\rm mol}$, in the entire Galaxy.

The left-hand panel of figure 3 shows two-dimensional (2D) distributions of the surface-density molecular fraction $f^{\Sigma}_{\rm mol}$, and the right-hand panel of figure 3 shows volume-density molecular fraction $f^{\rho}_{\rm mol}$ in the galactic plane at $Z = 0$. Figure 4 shows a vertical cross-section of the 3D $f^{\rho}_{\rm mol}$ map at $Y = 0$. Figure 5 shows sliced maps of $f^{\rho}_{\rm mol}$ distribution at different heights at every $\Delta Z = 40$ pc from $Z = -500$ pc to $+500$ pc.

Figures 3 and 4 show that the high-molecular-fraction region is located in the inner Galaxy at $R < \sim 8$ kpc, but the volume-density molecular fraction shows a much clearer plateau-like distribution. The edge of the plateau is called the molecular front, where the galactic scale phase transition from H I to H_2 is occurring.

2.3 Radial molecular front

Figure 6 shows radial variations of the volume densities of H I ($n_{\rm H\,I}$), H_2 ($2n_{H_2}$), and total gas density ($n_{\rm tot} = n_{\rm H\,I} + 2n_{H_2}$) in the galactic plane as a function of the galactocentric distance along the X-axis ($Y = 0$). In the figure, n(H) represents either $n_{\rm H\,I}$, $2n_{H_2}$, or $n_{\rm tot}$.

Figure 7 shows the corresponding volume-density molecular fraction , $f^{\rho}_{\rm mol}$. In addition, it shows the surface-density molecular fraction, $f^{\Sigma}_{\rm mol}$, in the (X, Z) plane calculated for the integrated column densities in Z-direction.

In the present analysis, we used densities along the X-axis at $Y = 0$ kpc, where kinematical distances, and therefore densities, are determined at better accuracy than along the Y-axis across the Sun.

The volume-density molecular fraction is as high as $f^{\rho}_{\rm mol} \sim 0.9$ at $R \leq 5$ kpc, and steeply decreases to low values less than 0.1 at $R > 9$ kpc with an e-folding radius interval of $\Delta R \sim 0.5$ kpc from $R = 7.5$ to 8 kpc. Figure 7 indicates that the high-molecular-fraction region forms a plateau-like disk with critical radius $R^{\rho}_{\rm F} \simeq 8$ kpc, where the fraction decreases sharply with radius, which we call the front radii.

On the other hand, the surface-density molecular fraction varies smoothly with the maximum value of about $f^{\Sigma}_{\rm mol} \sim 0.7$ at $R \leq 5$ kpc. Such a mild variation of $f^{\Sigma}_{\rm mol}$ is due to averaging effect of the thicker H I disk having smaller molecular fraction at high-Z regions as seen in figure 2.

The distribution of $f^{\Sigma}_{\rm mol}$ may be compared with those obtained for external galaxies. Similar front structure has been observed in nearby spiral galaxies (Sofue et al. 1995; Honma et al. 1995; Tanaka et al. 2014). A milder variation has been observed in later-type galaxies like M 33 (Tosaki

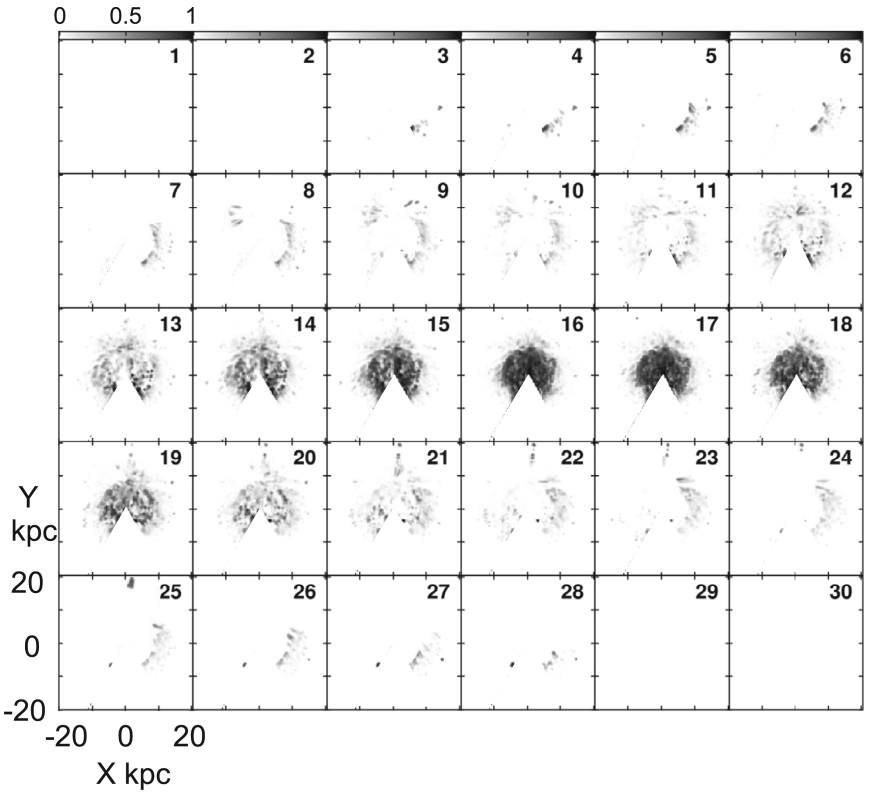

Fig. 5. Density molecular fraction $f^{\rho}_{\rm mol}$ at different heights Z from the galactic plane at 40-pc Z increments. The values are represented in gray-scale as indicated by the bar in the top left-hand corner.

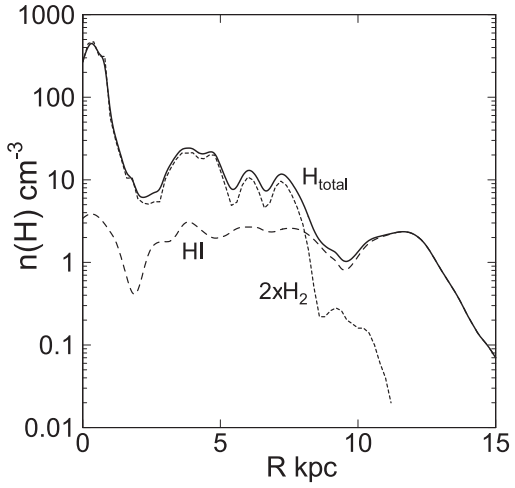

Fig. 6. Volume density n(H) ($= n_{\rm HI}, 2n_{\rm H_2}$, or $n_{\rm tot}$) plotted against R in the galactic plane along the X-axis.

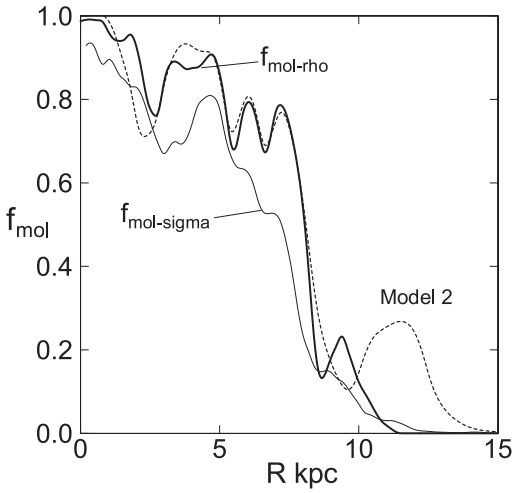

Fig. 7. $f^{\rho}_{\rm mol}$ (thick line) compared with $f^{\Sigma}_{\rm mol}$ (thin line) plotted against R. The dashed line shows a calculated curve based on the Elmegreen's (1993) model.

et al. 2011), where the maximum fraction was found to be about $f^{\Sigma}_{\rm mol} \simeq 0.22$ at $R \sim 0.6$ kpc.

It should be emphasized that the volume-density molecular fraction obtained here in the Milky Way shows a much clearer, sharper front behavior than those ever observed for surface molecular fraction in other galaxies.

2.4 Vertical molecular front

The 3D distribution of the molecular fraction makes it possible to examine the vertical variation of $f^{\rho}_{\rm mol}$ in detail. Figure 8 shows vertical variations of $f^{\rho}_{\rm mol}$ at different radii from $R = 0$ kpc at the Galactic center to $R = 14$ kpc at a galacto-centric longitude $\Theta = 45^{\circ}$. This figure indicates

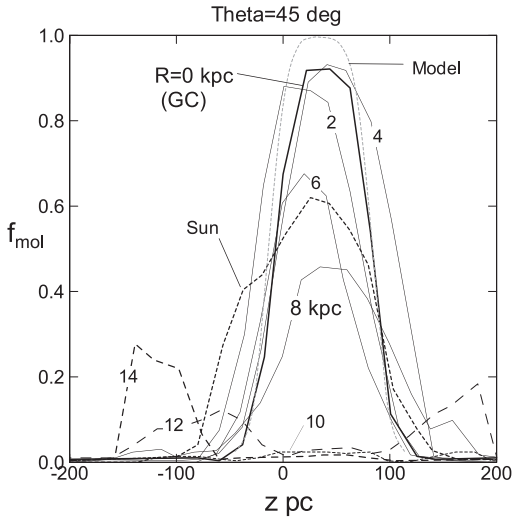

Fig. 8. Vertical variation of $f^{\rho}_{\rm mol}$ at $R = 0$ kpc (Galactic center), 2, 4, 6, 8, and Sun, 10, 12, and 14 kpc at a galacto-centric longitude $\Theta = 45^{\circ}$. The gray dotted line is a model curve. The vertical variation near the Sun ($R = 8$ kpc, $\Theta = 90^{\circ}$ is also indicated by the thick dashed line.

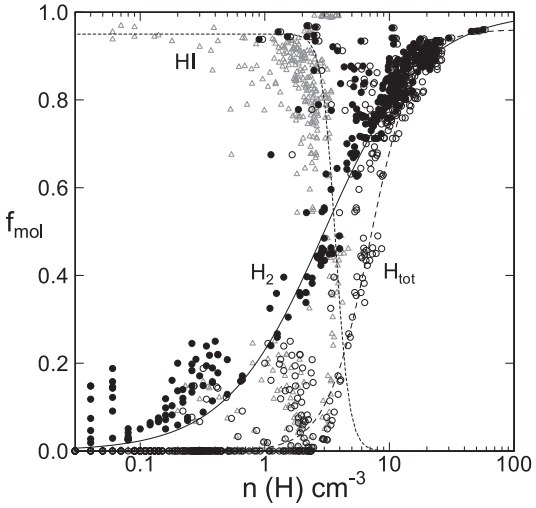

Fig. 9. $f^{\rho}_{\rm mol}$ plotted against densities of H I n(H I) (gray triangle), molecular hydrogen $2n(H_2)$ (filled circle), and total atomic hydrogen $n_{\rm total} = n({\rm H\,I}) + 2n(H_2)$ (open circle). The lines are approximate empirical fits as described in the text.

that the galactic disk inside the solar circle, particularly at ≤ 5 kpc, is molecular-gas dominant with $f^{\rho}_{\rm mol} \sim 0.8$–$0.93$ and as high as ~ 0.5 even near the solar circle. It then drastically decreases outside the solar circle.

It should be stressed that the $f^{\rho}_{\rm mol}$ decreases sharply with height at ± 50 pc from the midplane of maximum $f^{\rho}_{\rm mol}$, exhibiting the vertical molecular front of the molecular disk at $h_{\rm c} \simeq \pm 50$ pc. The shapes of the vertical and radial molecular fronts are similar, except for the scale radius and height.

2.5 Dependence of $f^{\rho}_{\rm mol}$ on the ISM density: Empirical law and H I threshold

It is known that the molecular gas is formed from and dissociated into H I gas responding to the interstellar condition. The molecular fraction is a function of the gas density through the pressure $P = n_{\rm tot} kT$, metallicity $\mathscr{Z}$, and UV radiation field intensity j (Elmegreen 1993), where $n_{\rm tot} = n_{\rm H\,I} + 2n_{\rm H_2}$, T is the equivalent ISM temperature, and k is the Boltzmann constant.

We now examine the dependence of $f^{\rho}_{\rm mol}$ on the densities, n(H). Figure 9 plots $f^{\rho}_{\rm mol}$ against n(H), where n(H) represents either $n_{\rm H\,I}$, $2n_{\rm H_2}$, or $n_{\rm tot}$.

The dependence of the molecular fraction on the gas densities can be represented by an empirical simple function as

$$f^{\rho}_{\rm mol} = \frac{f_{\rm max}}{1 + (n/n_{\rm c})^{\alpha}}, \tag{3}$$

where $n_{\rm c}$ is a critical density depending on the species.

This empirical law for total gas density is approximated by a parameter combination $f_{\rm max} = 0.96$, $n_{\rm c} = 7.0\,{\rm H\,cm^{-3}}$, and $\alpha = -2.5$, as shown by open circles in figure 9 and fitted by the dashed curve. The critical density of $7\,{\rm H\,cm^{-3}}$ is close to that of the molecular front in figure 7. The value may represent a threshold ISM density to generate the cold neutral medium (CNM) from the warm neutral medium (WNM) phase (Heiles & Troland 2003).

Table 1. Parameters for the empirical fit to n– $f^{\rho}_{\rm mol}$ plot in figure 9 by $f^{\rho}_{\rm mol} = f_{\rm max}/[1 + (n/n_{\rm c})^{\alpha}]$.

Phase	$f_{\rm max}$	$n_{\rm c}$ (H cm^{-3})	α
H I	0.95	3.7	+6
H_2	1.0	3.0	−1.1
$H_{\rm tot}$	0.96	7.0	−2.5

Similarly, $f^{\rho}_{\rm mol}$ depends on the molecular gas density by $f_{\rm max} = 1.0$, $n_{\rm c} = 3.0\,{\rm H\,cm^{-3}}$, and $\alpha = -1.1$, as shown by the filled circles fitted by the thin full line. Table 1 summarizes the parameters.

On the other hand, the dependence on the H I density (gray triangles in figure 9) is quite different. The dotted curve in figure 9 shows the same function for parameters $f_{\rm max} = 0.95$, $n_{\rm c} = 3.7\,{\rm H\,cm^{-3}}$, and $\alpha = +6$, representing a sharply dropping $f^{\rho}_{\rm mol}$ near an H I threshold value of $n_{\rm H\,I} \simeq 3.7\,{\rm H\,cm^{-3}}$. This implies that there is a maximum value of the mean H I density in the grids, each of a volume $200 \times 200 \times 20$ pc.

3 Comparison with theoretical models

The variation of $f^{\rho}_{\rm mol}$ in the R- and Z-directions can be calculated by a theoretical consideration of the phase transition in the interstellar gas taking account of the ISM pressure, P,

metallicity, $\mathscr{Z}$, and UV radiation field by stars, j (Elmegreen 1993; Tanaka et al. 2014).

We consider two cases of pressure distribution. In the first model (Model 1), the pressure P is expressed by an exponential function, and in the second semi-analytical model (Model 2) we adopt the observed total density distribution along the X-axis at $Z = 0$ and $Y = 0$ kpc as shown in figure 7. This direction was chosen for accurate densities than those along the Y-axis (Sun–Galactic center line), where the density is less certain for degenerated kinematic distances.

In Model 1 P is given by

$$P = P_0 e^{-(R-R_0)/R_P}, \tag{4}$$

where the scale radius is taken to be $R_P = 3$ kpc. In Model 2, the pressure P is assumed to be proportional to the observed total hydrogen density as

$$P = n_{\rm tot} kT. \tag{5}$$

We normalize the density by $n_{\rm tot:\,0} = 5.3\,{\rm cm}^{-3}$ from the present measurement at $R = X = 8$ kpc as an approximate representative value at the Sun. The temperature is assumed to be constant at $T = 7000$ K, equivalent to the velocity dispersion of clouds and interstellar turbulence, which is close to the pressure-equilibrium kinematic temperature, 8000 K, of the WNM (Heiles & Troland 2003). Note that the temperature is the equivalent temperature to kinetic energy (pressure), but not the excitation temperature. Here and hereafter, the suffix 0 denotes the values at $R = 8$ kpc approximately representing the solar value.

In both models, we adopt the same profiles for j and $\mathscr{Z}$ as

$$j = j_0 e^{-(R-R_0)/R_j} \tag{6}$$

and

$$\mathscr{Z} = \mathscr{Z}_0 e^{-(R-R_0)/R_Z}. \tag{7}$$

The radiation field is assumed to have the same scale radius as the pressure, $R_j = 3$ kpc, and the solar value, $j_0 = 0.8 \times 10^{-12}\,{\rm erg\,cm}^{-3}$ (Cox 2000), is the same as taken by Elmegreen (1993).

The metallicity gradient was determined by Shaver et al. (1983), who obtained $d\log\mathscr{Z}/dR = (-0.07 \pm 0.015)\,{\rm dex\,kpc}^{-1}$, where they assumed $R_0 = 10$ kpc. By rescaling the radius for $R_0 = 8$ kpc, the gradient can be rewritten as $d\log\mathscr{Z}/dR = (-0.7 \pm 0.15)/(8\,{\rm kpc})$, or $d\ln\mathscr{Z}/dR = -0.20 \pm 0.04\,{\rm kpc}^{-1} \simeq 1/(5 \pm 1\,{\rm kpc})$. This yields $R_Z \simeq 5$ kpc, and we adopt this value for equation (7).

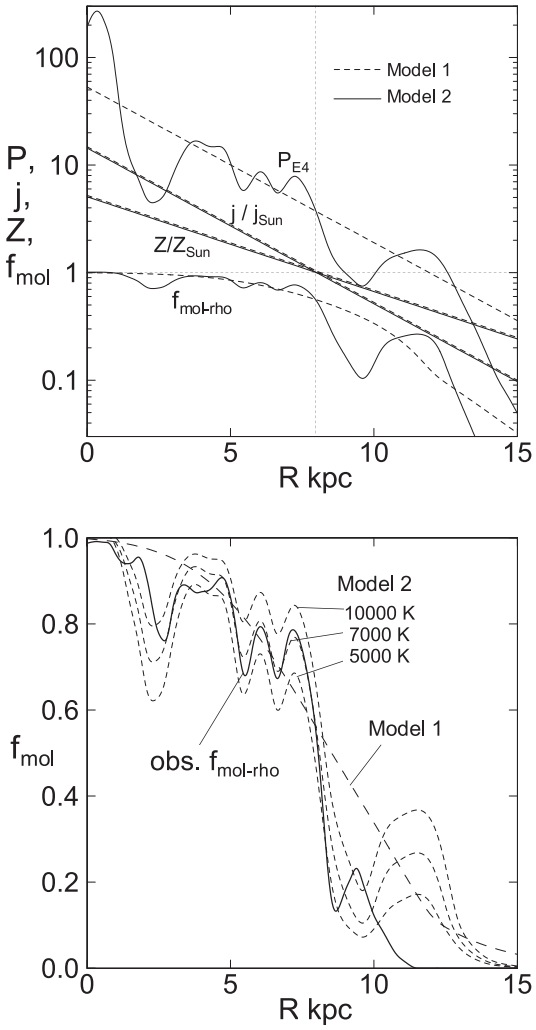

Fig. 10. (Top) Radial variations of $P_{\rm E4} = P/(10^4\,{\rm K\,cm}^{-3})$, j/j_0, $\mathscr{Z}/\mathscr{Z}_0$, and $f^{\rho}_{\rm mol}$ for Models 1 and 2 for $T = 7000$ K. (Bottom) Comparison of $f^{\rho}_{\rm mol}$ models with the observation (thick line): Model 1 for ISM temperature 7000 K (long-dashed line), and Model 2 for 5000, 7000, and 10000 K (dashed lines).

Calculated results for the two models using the code developed by Tanaka et al. (2014) based on the models of Elmegreen (1993) are shown in figures 7 and 10. The exponential model (Model 1) shows smooth and mild variation. Although it roughly approximates the general behavior of observed $f^{\rho}_{\rm mol}$, the sharp molecular front cannot be reproduced. On the other hand, the semi-analytical model (Model 2) using the observed density profile reproduces the observed $f^{\rho}_{\rm mol}$ well, when the ISM temperature is taken to be 7000 K. The model can reproduce not only the steep molecular front at $R \sim 8$ kpc but also the fluctuations.

The model profile is sensitive to the ISM temperature. If the temperature is changed to $\sim 10^4$ K or to ~ 5000 K, the fitting gets worse, with $f^{\rho}_{\rm mol}$ being increased or decreased significantly, as shown in figure 10. This implies that the

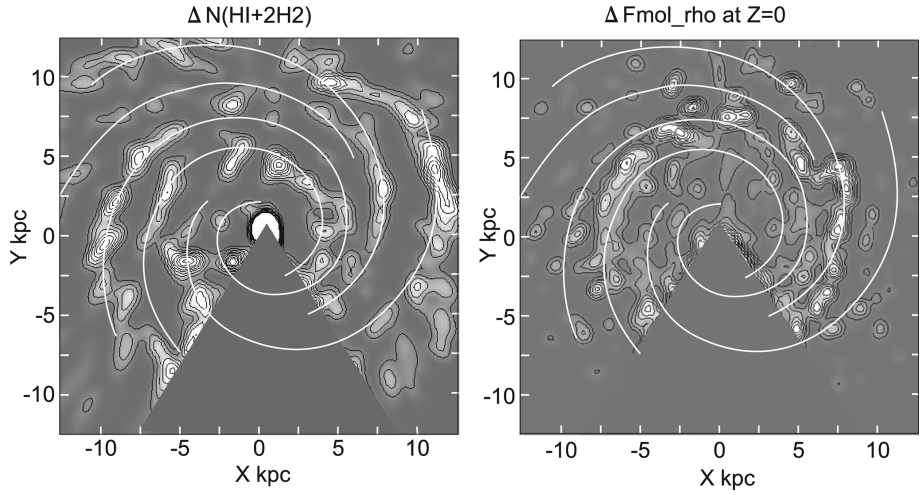

Fig. 11. Unsharp-masked total surface density ΔN(H I+2H$_2$) (left) and $\Delta f^{\rho}_{\rm mol}$ (right) maps. Contour interval for molecular fraction is 0.02. Spiral arms traced by Nakanishi and Sofue (2016) are indicated by white lines.

$f^{\rho}_{\rm mol}$ fitting can be used to determine the ISM temperature, if the radiation field and metallicity are given.

The Z-directional density profile is expressed by a hyperbolic cosecant function of the height Z. The metallicity and the radiation intensity field are expressed by an exponentially decreasing function with R and Z. The Z-directional variation of model $f^{\rho}_{\rm mol}$ is shown in figure 8 for the inner region of the Galaxy. The steep vertical variation of $f^{\rho}_{\rm mol}$ near the vertical molecular front is reproduced well by this model.

4 Spiral arms

In order to see the variation of molecular fraction in relation to the spiral arms, we made an unsharp-masked map of the density molecular fraction in the galactic plane. The original map was smoothed by a Gaussian beam with full width of 5 pixels, or 1 kpc, and the smoothed map was subtracted from the original to yield a difference map, $\Delta f^{\rho}_{\rm mol}$. The obtained difference (unsharp-masked) map is shown in figure 11, displaying only positive $\Delta f^{\rho}_{\rm mol}$ regions. It is also compared with an unsharp-masked map of the total gas density for the same masking parameters. The spiral arms traced in our earlier works are superposed by white lines (Nakanishi & Sofue 2006, 2016).

We stress that the $\Delta f^{\rho}_{\rm mol}$ map exhibits spiral arms at radii $R \sim 6$ to 10 kpc near the molecular front. A clear coincidence is found with the Perseus arm, where the $f^{\rho}_{\rm mol}$ arm almost perfectly traces the spiral arm. However, $\Delta f^{\rho}_{\rm mol}$ arms are hardly seen in the innermost region at $R < \sim 5$ kpc, where the molecular fraction is saturated close to unity, and molecular clouds travel through the interarm regions without being dissociated into H I (Koda et al. 2016). Also in the outer Galaxy at $R > \sim 10$ kpc, where the gas is almost totally H I, $\Delta f^{\rho}_{\rm mol}$ arm is not present generally.

Hence, in the transition region at $R = 6$ to 10 kpc, molecular clouds are formed within the spiral arms, and are dissociated in the interarm region. This is consistent with the long arm–interarm crossing time of the spiral pattern,

$$t \sim \pi/(\Omega - \Omega_{\rm p}), \tag{8}$$

which is on the order of $\sim$ several $\times$ 10^8–10^9 yr and is sufficiently longer than the molecular gas formation time scale $t_{\rm mol} \sim 10^7$ yr (Goldsmith et al. 2007). Here, $\Omega = V_{\rm rot}/R \sim 20\,{\rm km\,cm^{-1}\,kpc^{-1}}$ is the angular velocity of the disk gas for $V_{\rm rot} = 220\,{\rm km\,s^{-1}}$ and $R = 8$–10 kpc, and $\Omega_{\rm p} \sim 23\,{\rm km\,cm^{-1}\,kpc^{-1}}$ (Junqueira et al. 2015) is the pattern speed.

Besides these $f^{\rho}_{\rm mol}$ arms, there is a particular region near $(X, Y) \sim (-5, +5)$ kpc between the Scutum–Crux and Sagittarius–Carina arms, where $f^{\rho}_{\rm mol}$ is enhanced in the interarm region. However, this was due to the sharp edge of the molecular front in this area which caused an artifact of arm-like enhancement when the unsharp-masking was applied.

5 Summary and discussion

5.1 3D sharp molecular fronts

We constructed a 3D cube of the volume-density molecular fraction, $f^{\rho}_{\rm mol}$, using the H I and H$_2$ density cubes of the Milky Way. The radial molecular front in the galactic plane observed in the density molecular fraction $f^{\rho}_{\rm mol}$ is found to be sharper than that for the surface density molecular fraction $f^{\Sigma}_{\rm mol}$. The molecular front of $f^{\rho}_{\rm mol}$ is also found in the vertical direction.

Plots of $f^{\rho}_{\rm mol}$ against H I, H_2, and total gas densities showed that $f^{\rho}_{\rm mol}$ is a function of gas densities empirically expressed by equation (3). A threshold value was obtained in the H I density at $n_{\rm H\,I} \simeq 3.7\,{\rm H\,cm^{-3}}$, above which the gas is transformed almost totally into molecular gas.

5.2 Reproduction by theoretical models

The radial and Z-directional variations of the observed $f^{\rho}_{\rm mol}$ and sharp molecular fronts are reproduced well by the theoretical calculations using Elmegreen's (1993) model. We showed that the radial profile is a sensitive function of the ISM temperature, which was here taken to be 7000 K for reasonable fitting. The temperature is consistent with the pressure-equilibrium kinetic temperature, 8000 K, derived for the warm neutral ISM (Heiles & Troland 2003).

The radial $f^{\rho}_{\rm mol}$ profile was analyzed only along the $+Y$-axis because of the highest quality of data around this direction as seen in figures 1 and 3. The profile may represent the typical radial variation in the whole galaxy, and analyses along other radial directions will give almost the same result. Also, azimuthal averaging was not applied, as it smears out the molecular fronts to be studied in this paper due to the globally asymmetric distribution of the gases (figure 1).

5.3 Enhanced-$\Delta f^{\rho}_{\rm mol}$ spiral arms

A 2D unsharp-masked $\Delta f^{\rho}_{\rm mol}$ map in the galactic plane exhibited spiral arms with enhanced molecular fraction at $R \sim 6$ to 10 kpc near the molecular front. A clear $f^{\rho}_{\rm mol}$ arm was found that coincided with the Perseus arm. This fact implies that H I gas is transformed into molecular gas along a spiral arm with marginal $f^{\rho}_{\rm mol}$ near the molecular front (transition region). However, no clear $f^{\rho}_{\rm mol}$ arms are seen at $R < 6$ kpc or at $R > 10$ kpc, where the gas is either totally molecular or H I. In extragalactic systems, an enhancement of $f^{\Sigma}_{\rm mol}$ has been observed in outer spiral arms of the Sb galaxy M 51 (Hidaka & Sofue 2002).

5.4 Effects of cold/opaque H I and dark H_2 gases

If we consider cold H I gas, it may increase the total H I density by a factor of ~2 (Fukui et al. 2015). Moreover, if we consider the finite optical thickness, the H I densities, which have been calculated upon an optically thin assumption, will be increased. By increasing the H I density, $f_{\rm mol}$ will generally decrease, and the molecular front will be shifted toward inside. Similarly, CO-free "dark" H_2 gas has been suggested (Wolfire et al. 2010), which might also affect the result. Detailed discussions of the effects of cold/opaque H I and dark molecular gases are, however, beyond the scope of this paper.

Acknowledgments

The authors are indebted to Prof. K. Kohno of IoA, the University of Tokyo, for his support during the work.

References

Bolatto, A. D., Wolfire, M., & Leroy, A. K. 2013, ARA&A, 51, 207
Cox, A. N. ed. 2000, Allen's Astrophysical Quantities, 4th ed. (New York: Springer), ch. 23
Dame, T. M., Hartman, D., & Thaddeus, P. 2001, ApJ 547, 792
Elmegreen, B. G. 1993, ApJ, 411, 170
Fukui, Y., Torii, K., Onishi, T., Yamamoto, H., Okamoto, R., Hayakawa, T., Tachihara, K., & Sano, H. 2015, ApJ, 798, 6
Goldsmith, P. F., Li, D., & Krčo, M. 2007, ApJ, 654, 273
Heiles, C., & Troland, T. H. 2003, ApJ, 586, 1067
Hidaka, M., & Sofue, Y. 2002, PASJ, 54, 223
Honma, M., Sofue, Y., & Arimoto, N. 1995, A&A, 304, 1
Imamura, K., & Sofue, Y. 1997, A&A, 319, 1
Junqueira, T. C., Chiappini, C., Lépine, J. R. D., Minchev, I., & Santiago, B. X. 2015, MNRAS, 449, 2336
Kalberla, P. M. W., Burton, W. B., Hartmann, D., Arnal, E. M., Bajaja, E., Morras, R., & Pöppel, W. G. L. 2005, A&A, 440, 775
Koda, J., Scoville, N., & Heyer, M. 2016, ApJ, 823, 76
Krumholz, M. R., McKee, C. F., & Tumlinson, J. 2009, ApJ, 693, 216
Nakanishi, H., et al. 2006, ApJ, 651, 804
Nakanishi, H., & Sofue, Y. 2003, PASJ, 55, 191
Nakanishi, H., & Sofue, Y. 2006, PASJ, 58, 847
Nakanishi, H., & Sofue, Y. 2016, PASJ, 68, 5
Shaver, P. A., McGee, R. X., Newton, L. M., Danks, A. C., & Pottasch, S. R. 1983, MNRAS, 204, 53
Sofue, Y., Honma, M., & Arimoto, N. 1995, A&A, 296, 33
Tanaka, A., Nakanishi, H., Kuno, N., & Hirota, A. 2014, PASJ, 66, 66
Tosaki, T., et al. 2011, PASJ, 63, 1171
Wolfire, M. G., Hollenbach, D., & McKee, C. F. 2010, ApJ, 716, 1191